



1 **Towards understanding the intrinsic variations of the Priestley-Taylor**  
2 **coefficient based on a theoretical derivation**

3 Ziwei Liu, Hanbo Yang \*, Changming Li, Taihua Wang

4 State Key Laboratory of Hydro-science and Engineering, Department of Hydraulic  
5 Engineering, Tsinghua University, Beijing, China

6 *Correspondence to:* Hanbo Yang (yanghanbo@tsinghua.edu.cn)



## 7 **Abstract**

8 Priestley-Taylor (PT) coefficient ( $\alpha$ ) is generally set as a constant value or fitted as an  
9 empirical function of environmental variables, and it can bias the evaporation estimation  
10 or hydrological projections. This study derives a theoretical equation for  $\alpha$  using an  
11 atmospheric boundary layer model, which shows that  $\alpha$  is a function of air temperature  
12 (T) and specific humidity (Q). More importantly, the derived expressions can well  
13 estimate the sensitivity of  $\alpha$  to T and Q, that is,  $d\alpha/dT$  and  $d\alpha/dQ$ , compared to water  
14 surface observations.  $\alpha$  is generally negatively associated with T and Q, and its changes  
15 are fundamentally controlled by T and modulated by Q. Based on climate model data, it  
16 is shown that the variation of  $\alpha$  to T (negative association) is of great importance for long-  
17 term hydrological predictions. For practical and broad uses, a lookup graph is also  
18 provided to directly find the  $d\alpha/dT$  and  $d\alpha/dQ$  values. Overall, the derived expression  
19 gives a physically clear and straightforward approach to quantify changes in  $\alpha$ , which is  
20 essential for PT-based hydrological simulation and projections.

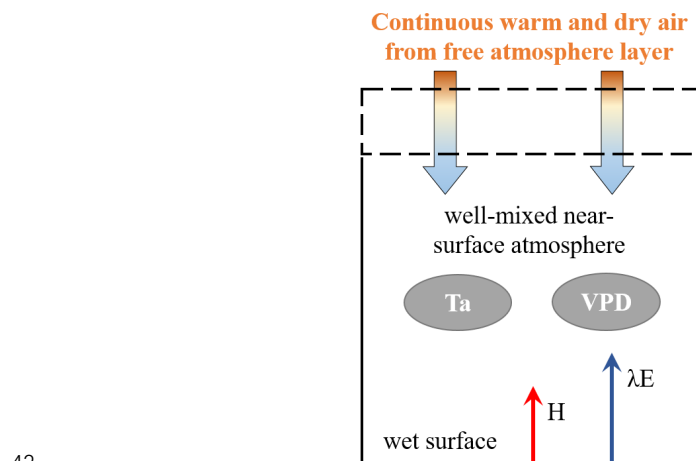


## 21 1. Introduction

22 Evaporation from wet surfaces, including oceans, lakes, and reservoirs, is relevant to  
23 global hydrological cycles and water availability. There is a long history of developing  
24 theories and methods to estimate wet surface evaporation (Bowen, 1926; Penman, 1948;  
25 Priestley and Taylor, 1972; Thornthwaite and Holzman, 1939; Yang and Roderick, 2019).  
26 Among existing models, the Priestley-Taylor (PT) model/equation is known for its  
27 transparent structure and low input requirement (Priestley and Taylor, 1972). The PT  
28 equation is widely used in evaporation estimation across varied scales and is the basis for  
29 various hydrologic and land surface models. Specifically, the PT equation comes from  
30 the equilibrium evaporation ( $\lambda E_{eq}$ ), and  $\lambda E_{eq}$  can be calculated as (Slatyer and McIlroy,  
31 1961):

$$32 \lambda E_{eq} = \frac{\epsilon_a}{\epsilon_a + 1} (R_n - G) \quad (1)$$

33 where  $\lambda$  is the latent heat of water vaporization,  $\epsilon_a = \Delta/\gamma$ ,  $\Delta$  is the slope of the saturated  
34 vapor pressure versus temperature curve (a function of temperature), and  $\gamma$  is the  
35 psychrometric constant.  $\epsilon_a$  is a function of air temperature (T).  $R_n - G$  is the available  
36 energy. The equilibrium condition indicates that the near-surface air is saturated,  
37 supposing the vapor pressure deficit (VPD) is zero. However, it does not exist in the real  
38 world (Brutsaert and Stricker, 1979; Lhomme, 1997a), due to the continuous exchanges  
39 of warm and dry airs from the entrainment layer, although water is continuously  
40 transported from the bottom wet surface into the atmosphere through evaporation process  
41 (Figure 1).



42

43 Figure 1. Atmospheric boundary layer box model describing the energy and water fluxes  
44 at the saturated surface and atmosphere above. The dotted line represents the removable  
45 upper boundary of the box.  $H$  and  $\lambda E$  are the sensible and latent heat fluxes.  $T_a$  is the air



46 temperature and VPD is the vapor pressure deficit.

47

48 In this case, the PT equation introduced a parameter,  $\alpha$ , known as the PT coefficient, to  
49 estimate wet surface evaporation (Priestley and Taylor, 1972).  $\alpha$  includes the effects of  
50 vertical mixing of dry and moist air, and adjusts the equilibrium evaporation to the actual  
51 evaporation. So qualitatively speaking, the  $\alpha$  is impossibly lower than one because the air  
52 is always not saturated and can only infinitely close to saturated condition, no matter how  
53 moist the near-surface air is. The PT equation is:

$$44 \quad \lambda E = \alpha \frac{\epsilon_a}{\epsilon_a + 1} (R_n - G) \quad (2)$$

55 In the original study of Priestley and Taylor (1972), the value of  $\alpha$  is  $\sim 1.26$ . With the fixed  
56  $\alpha$  value of 1.26, the PT model can reasonably estimate wet surface evaporation (Yang and  
57 Roderick, 2019). But concurrently, some studies found  $\alpha$  often shows a more prominent  
58 value under cold conditions and becomes lower as warms (Debruin and Keijman, 1979;  
59 Xiao *et al.*, 2020). This indicates that  $\alpha$  should not be a constant in space and time (Maes  
60 *et al.*, 2019). Logically, this value would change with environmental conditions, such as  
61 changes in temperature, humidity, advection, and dry-air entrainment (Assouline *et al.*,  
62 2016; Crago *et al.*, 2023; Eichinger *et al.*, 1996; Guo *et al.*, 2015; Jury and Tanner, 1975;  
63 Lhomme, 1997b; McNaughton and Spriggs, 1986; van Heerwaarden *et al.*, 2009). A  
64 general method for connecting  $\alpha$  to external factors is to inverse  $\alpha$  with observations based  
65 on Equation (2) and then build relationships among  $\alpha$  and investigated variables. A  
66 negative relationship between  $\alpha$  and temperature (T) is a consensus from multi-scale  
67 observations (Assouline *et al.*, 2016; Xiao *et al.*, 2020). Thus from the practical  
68 perspective, many attempts empirically fitted  $\alpha$  as a function of temperature (Andreas and  
69 Cash, 1996; Hicks and Hess, 1977; Yang and Roderick, 2019). Recent work further  
70 showed that the air humidity state also plays a role in  $\alpha$  changes (Su and Singh, 2023).  
71 Those findings help us to know how  $\alpha$  changes with external conditions. However, most  
72 works are on the empirical side and more about observed phenomena. Meanwhile,  
73 regarding physical understandings for  $\alpha$ , there still remain some questions, for example,  
74 why  $\alpha$  and T negatively correlate, how the interaction between temperature and air  
75 humidity affects  $\alpha$ , and whether  $\alpha$  has a lower boundary as it is negatively associated with  
76 temperature.

77 Based on a recent study (Liu and Yang, 2021), here we derived an explicit and physically  
78 clear equation to quantify relationships among  $\alpha$ , T, and Q. The derived expression can  
79 be used to estimate the sensitivity of  $\alpha$  to T and Q. In the following sections, we will first  
80 provide the theory for estimating  $\alpha$  and its sensitivity to T and Q, then we evaluate the  
81 theory based on measured data, followed by an analysis of the influences of  $\alpha$  changes on  
82 long-term hydrologic projections.



## 83 2. Theory

### 84 2.1 Derivation of Bowen ratio

85 Here, we use an atmospheric boundary layer-based (ABL) model as the basis for the  
86 Bowen ratio (defined as the ratio of sensible heat fluxes to latent heat fluxes,  $H/\lambda E$ )  
87 derivation (Liu and Yang, 2021). The fundamental conservation equations for states of  
88 moisture and energy over the water surfaces are (Raupach, 2001):

$$89 \quad \rho c_p \frac{d\theta}{dt} = \frac{H}{h} + \frac{\rho c_p g_e}{h} (\theta_e - \theta) \quad (3)$$

$$90 \quad \rho \lambda \frac{dQ}{dt} = \frac{\lambda E}{h} + \frac{\rho \lambda g_e}{h} (Q_e - Q) \quad (4)$$

91 where  $\theta$  is the potential temperature,  $Q$  is the specific humidity,  $c_p$  is the specific heat  
92 capacity of air at constant pressure,  $g_e$  is the entrainment flux velocity into the ABL box,  
93 and  $h$  is the height of the ABL. The subscript  $e$  indicates the variable is evaluated at the  
94 upper boundary of the ABL (see Figure 1).

95 According to Equations (3) and (4), we can obtain a formula to calculate the rate of VPD  
96 ( $dVPD/dt$ , see details in Liu and Yang (2021)):

$$97 \quad \frac{dVPD}{dt} = \frac{\varepsilon_a H - \lambda E}{\rho \lambda h} + \frac{g_e}{h} \Delta_D \quad (5)$$

98 where  $\Delta_D$  is calculated as:

$$99 \quad \Delta_D = VPD_e - VPD \quad (6)$$

100 Under the equilibrium state, the water vapor is continuously transported from the water  
101 surface to the atmosphere, keeping the air saturated. In this case, there is no vertical  
102 moisture gradient, that is, the air near the surface and the air at the upper boundary of the  
103 ABL should be saturated, so VPD and  $VPD_e$  are both equal to zero. With Equation (6),  
104 we can know  $\Delta_D = 0$ .

105 Under the non-equilibrium state, the air is not saturated, we can rewrite Equation (6) as:

$$106 \quad \Delta_D = Q - Q_e + [Q_{sat}(\theta_e) - Q_{sat}(\theta)] \quad (7)$$

107 where  $Q_e$  is much smaller than  $Q$ , and  $Q_{sat}(\theta_e) - Q_{sat}(\theta)$  is small (one order of magnitude  
108 smaller than  $Q$ ), so the  $\Delta_D$  roughly equals  $Q$  (Liu and Yang, 2021; Raupach, 2001).

109 Under a relatively long-term (monthly and/or longer), there is a potential VPD budget



110 (dVPD/dt = 0) over water surfaces (Raupach, 2001), and  $g_e$  can be estimated as the  
 111 function of H and  $\lambda E$  as:

$$112 \quad g_e = \frac{H + \Lambda \cdot \lambda E}{\rho c_p \gamma_v h} \quad (8)$$

113 where  $\Lambda$  is a constant (0.07), and  $\gamma_v$  is the potential virtual temperature gradient in the  
 114 free atmosphere above the ABL.  $\gamma_v h$  can be set as a fixed value of 7 K (Liu and Yang,  
 115 2021). Combining with the VPD budget, Equation (5) and (8), we can obtain the  
 116 expression for Bo:

$$117 \quad Bo = \begin{cases} \frac{1}{\epsilon_a}, \text{equilibrium} \\ \frac{1 - \Lambda \chi}{\epsilon_a + \chi}, \text{non-equilibrium} \end{cases} \quad (9)$$

118 where  $\chi = \frac{\lambda Q}{c_p \gamma_v h}$ , a function of Q.

## 119 2.2 Theoretical formula for $\alpha$

120 The surface energy balance is expressed as:

$$121 \quad R_n = H + \lambda E + G = (1 + Bo)\lambda E + G. \quad (10)$$

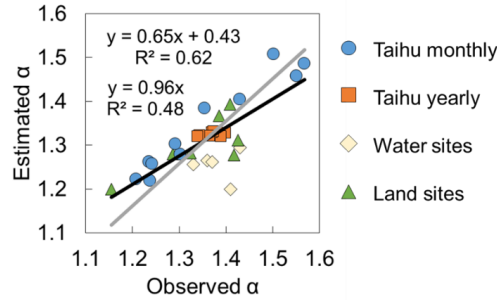
122 Combining Equations (2) and (10),  $\alpha$  can be calculated as:

$$123 \quad \alpha = \frac{1}{1 + Bo} \frac{\epsilon_a + 1}{\epsilon_a}. \quad (11)$$

124 With Equation (9) and (11), we can derive the formula for  $\alpha$ :

$$125 \quad \alpha = \begin{cases} 1, \text{equilibrium} \\ 1 + \frac{(\epsilon_a \Lambda + 1)\chi}{\epsilon_a [\epsilon_a + 1 + (1 - \Lambda)\chi]}, \text{non-equilibrium} \end{cases} \quad (12)$$

126 Equation (12) is one of the main results in this study, and it can estimate  $\alpha$  well compared  
 127 to a large number of observations (Figure 2, please see the description of observed data  
 128 in Section 3).



129

130 Figure 2. Comparison between observed and Equation (12) calculated  $\alpha$ . The black line  
 131 is the linear fitting with intercept and the gray line is the linear fitting through origin. The  
 132 observed  $\alpha$  is inversed by the PT model.

### 133 2.3 The sensitivity of $\alpha$ to air temperature and humidity

134 According to the above derivations, we can know that  $\alpha$  is not a constant and it changes  
 135 with T and Q. The sensitivity of  $\alpha$  to T and Q,  $d\alpha/dT$  and  $d\alpha/dQ$ , determines the variation  
 136 of  $\alpha$  if the initial  $\alpha$  value is given. In this section, we derive explicit equations to estimate  
 137  $d\alpha/dT$  and  $d\alpha/dQ$ .

138 Firstly, we decompose  $\alpha$  changes in that of T and Q with partial differential equations  
 139 based on Equation (11):

$$140 \quad \frac{\partial \alpha}{\partial T} = -\frac{1}{(1 + Bo_{ABL})^2} \frac{\epsilon_a + 1}{\epsilon_a} \frac{\partial Bo_{ABL}}{\partial T} - \frac{1}{\epsilon_a^2} \frac{1}{1 + Bo_{ABL}} \frac{\partial \epsilon_a}{\partial T}, \quad (13)$$

$$141 \quad \frac{\partial \alpha}{\partial Q} = -\frac{1}{(1 + Bo_{ABL})^2} \frac{\epsilon_a + 1}{\epsilon_a} \frac{\partial Bo_{ABL}}{\partial Q}, \quad (14)$$

142 where  $\frac{\partial Bo_{ABL}}{\partial T}$  and  $\frac{\partial Bo_{ABL}}{\partial Q}$  can be estimated based on Equation (9) as:

$$143 \quad \frac{\partial Bo_{ABL}}{\partial T} = -\frac{1 - \Lambda \chi}{(\epsilon_a + \chi)^2} \frac{\partial \epsilon_a}{\partial T}, \quad (15)$$

$$144 \quad \frac{\partial Bo_{ABL}}{\partial Q} = -\frac{\Lambda \epsilon_a + 1}{(\epsilon_a + \chi)^2} \frac{\partial \chi}{\partial Q}. \quad (16)$$

145 where terms of  $\frac{\partial \epsilon_a}{\partial T}$  and  $\frac{\partial \chi}{\partial Q}$  can be approximated as:

$$146 \quad \frac{\partial \epsilon_a}{\partial T} = \frac{1}{\gamma} \frac{\partial \Delta}{\partial T}, \quad (17)$$



$$147 \quad \frac{\partial \chi}{\partial Q} = \frac{\lambda}{c_p \gamma_v h}, \quad (18)$$

148 where  $\Delta$  can be calculated as:

$$149 \quad \Delta = \frac{4098 e_s}{(T + 237.3)^2}. \quad (19)$$

150 Combining Equation (13)-(18), we can obtain:

$$151 \quad \frac{\partial \alpha}{\partial T} = \frac{1}{\gamma} \left[ \frac{1}{(1 + \text{Bo}_{\text{ABL}})^2} \frac{1 - \Lambda \chi}{(\epsilon_a + \chi)^2} \frac{\epsilon_a + 1}{\epsilon_a} - \frac{1}{\epsilon_a^2} \frac{1}{1 + \text{Bo}_{\text{ABL}}} \right] \frac{\partial \Delta}{\partial T} \quad (20)$$

$$152 \quad \frac{\partial \alpha}{\partial Q} = \frac{1}{(1 + \text{Bo}_{\text{ABL}})^2} \frac{\Lambda \epsilon_a + 1}{(\epsilon_a + \chi)^2} \frac{\epsilon_a + 1}{\epsilon_a} \frac{\lambda}{c_p \gamma_v h} \quad (21)$$

153 We can rewrite the Equation (20) as follows:

$$154 \quad \frac{\partial \alpha}{\partial T} = -\frac{1}{\gamma} \frac{\chi [\epsilon_a (\Lambda \epsilon_a + 2) + \chi (1 - \Lambda) + 1]}{(1 + \text{Bo}_{\text{ABL}})^2 (\epsilon_a + \chi)^2 \epsilon_a^2} \frac{\partial \Delta}{\partial T}, \quad (22)$$

155 The total differentiation of  $\alpha$  is:

$$156 \quad d\alpha = \frac{\partial \alpha}{\partial T} dT + \frac{\partial \alpha}{\partial Q} dQ, \quad (23)$$

157 thus  $\frac{d\alpha}{dT}$  and  $\frac{d\alpha}{dQ}$  can be written as:

$$158 \quad \frac{d\alpha}{dT} = \frac{\partial \alpha}{\partial T} + \frac{\partial \alpha}{\partial Q} \frac{dQ}{dT}, \quad (24)$$

$$159 \quad \frac{d\alpha}{dQ} = \frac{\partial \alpha}{\partial Q} + \frac{\partial \alpha}{\partial T} \frac{dT}{dQ}. \quad (25)$$

160 With the above equations, we can get theoretical relationships among  $\alpha$ , T, and Q. This  
 161 derivation can provide a simple and physically clear estimation for  $\alpha$  changes. We also  
 162 obtained  $d\alpha/dT$  and  $d\alpha/dQ$  values by fitting measured data using the linear regression  
 163 model.

164 For practical use, we simplified the Equation (20) and (21) as:

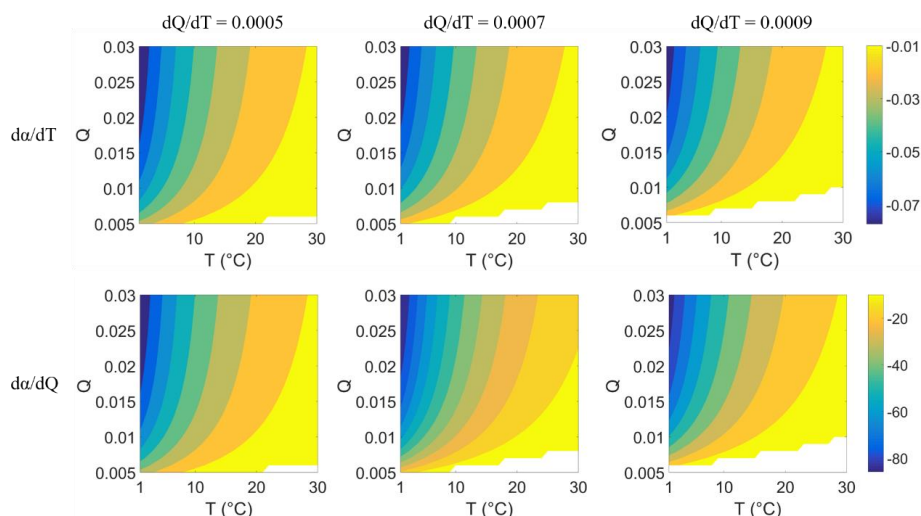
$$165 \quad \frac{\partial \alpha}{\partial T} = -\frac{1}{\gamma} \frac{\chi}{\epsilon_a} \frac{1}{\epsilon_a + \chi} \frac{1}{\epsilon_a^2} \frac{\partial \Delta}{\partial T} \quad (26)$$

$$166 \quad \frac{\partial \alpha}{\partial Q} = \frac{\epsilon_a + 1}{\epsilon_a (\epsilon_a + \chi + 1)^2} \frac{\chi}{Q} \quad (27)$$

167 We further gave a numerical plot to show how  $\alpha$  changes with T and Q (Figure 3). We  
 168 plot this figure by setting a  $dQ/dT$  gradient from 0.0005, 0.0007, and 0.0009/K to ensure  
 169 cover most of the cases over water surfaces. Figure 3 can be used as the lookup graphs to  
 170 directly find  $d\alpha/dT$  and  $d\alpha/dQ$  values. For example, for a water surface with  $dQ/dT$



171 about 0.0007 /K, the values of  $da/dT$  and  $da/dQ$  can be found in the second column  
172 of Figure 3.



173

174 Figure 3. Values of  $da/dT$  and  $da/dQ$  under different T and Q. The first and second  
175 rows are  $da/dT$  and  $da/dQ$ , respectively. The first to third columns are under different  
176 correlations between Q and T ( $dQ/dT$ ) as 0.0005, 0.0007, and 0.0009/K, respectively.  
177 The blank space in each subpanel refers to values of  $da/dT$  and  $da/dQ$  are negative,  
178 indicating situations that rarely happen in the real world (i.e., with a very high temperature,  
179 the specific humidity is hardly deficient over wet surfaces).

### 180 3. Cases and applications

#### 181 3.1 Data

182 We select data from eddy covariance measurements on several water surfaces (Han and  
183 Guo, 2023): (i) Lake Taihu, located in the Yangtze River Delta, China, with an area of  
184  $\sim 2,400$  km<sup>2</sup>, an average depth of 1.9 m (Lee *et al.*, 2014). There are five sites over the  
185 Taihu surface, and the poor-quality data marked with quality flags are removed. (ii) Lake  
186 Poyang, located in the Yangtze Plain, China, with an area of  $\sim 3,000$  km<sup>2</sup> and an average  
187 depth of 8.4 m (Zhao and Liu, 2018). (iii) Erhai, located in the Yun-Gui Plateau of China,  
188 with an area of  $\sim 250$  km<sup>2</sup> and an average depth of 10 m (Du *et al.*, 2018). (iv) Guandu  
189 Ponds, located in Anhui Province, China, with an area of  $\sim 0.05$  km<sup>2</sup> and an average depth  
190 of 0.8 m (Zhao *et al.*, 2019); (v) Lake Suwa, located in Nagano, Japan, with an area of  
191  $\sim 13$  km<sup>2</sup> and an average depth of 4 m (Taoka *et al.*, 2020). Months with negative values  
192 of sensible heat fluxes have not remained. The latitude, longitude, and available data  
193 period of five lakes/ponds are listed in Table 1. For  $\alpha$  changes in time, we use data from



194 Lake Taihu for investigation due to its sufficient data length. For  $\alpha$  changes in space, we  
195 calculate the average temperature, specific humidity, and  $\alpha$  of each lake for comparison.

196 Table 1. Location and date period of each water body.

Site	Lat (°)	Lon (°)	Size (km <sup>2</sup> )	Periods <sup>a</sup>	Sample size (number of months)
Taihu	31.23	120.11	3000	2012.01 - 2018.12	341 <sup>b</sup>
Poyang	29.08	116.40	2400	2013.08 - 2017.09	41
Erhai	25.77	100.17	250	2012.01 - 2018.12	24 <sup>c</sup>
Guandu	31.97	118.25	0.05	2017.06 - 2019.12	31
Suwa	36.05	138.11	13	2016.01 - 2018.12	36

197 Note: a. Periods refer to the date of the first measurement to the date of the last one,  
198 including months for which no data are available. b. There are five eddy covariance sites  
199 over lake Taihu. c. Only climatology monthly data from two periods of 2012-2015 and  
200 2015-2018 are available.

201 Observations from global flux sites (FluxNet2015 database) are also selected. We first  
202 examine days without water stress based on the following steps (Maes *et al.*, 2019). At  
203 each site, the evaporative fraction EF (i.e., latent heat flux over the sum of latent and  
204 sensible fluxes) is first calculated, and the days with EF exceeding the 95th percentile EF  
205 and with EF larger than 0.8 remain. Secondly, the days with soil moisture lower than 50%  
206 of the maximum soil moisture (taken as the 98th percentile of the soil moisture series) are  
207 removed. Days having rainfall and negative values of latent and sensible heat fluxes are  
208 also not included. As a result, a total of ~700 non-water-stressed site-days pass the  
209 criterion. Data is divided into seven vegetation types including croplands (CRO),  
210 wetlands (WET), evergreen needleleaf and mixed forests (DNF\_MF), evergreen  
211 broadleaf and deciduous broadleaf forests (EBF\_DBF), grasslands (GRA), close  
212 shrublands (CSH), and woody savanna (WSA), to analyze  $\alpha$  changes in space.

213 We also collect ocean surface data from 11 CMIP6 models (under scenario SSP585, Table  
214 2) from 2021-2100 to see the temporal changes in  $\alpha$ . The calculation is limited to the  
215 latitudinal range 60°S to 60°N, and takes all ocean surface grids as a whole (Roderick *et*  
216 *al.*, 2014). We average the monthly data to the yearly scale and calculate  $\alpha$  every ten years  
217 from 2021 to 2100 (i.e., 2021-2030, 2031-2040, etc.).

218 Table 2. CMIP6 models used in this study.

Model	Nation	Institute
ACCESS-ESM1-5	Australia	CSIRO
CanESM5	Canada	CCCma
CESM2-WACCM	USA	NCAR
CMCC-CM2-SR5	Italy	CMCC
CMCC-ESM2	Italy	CMCC

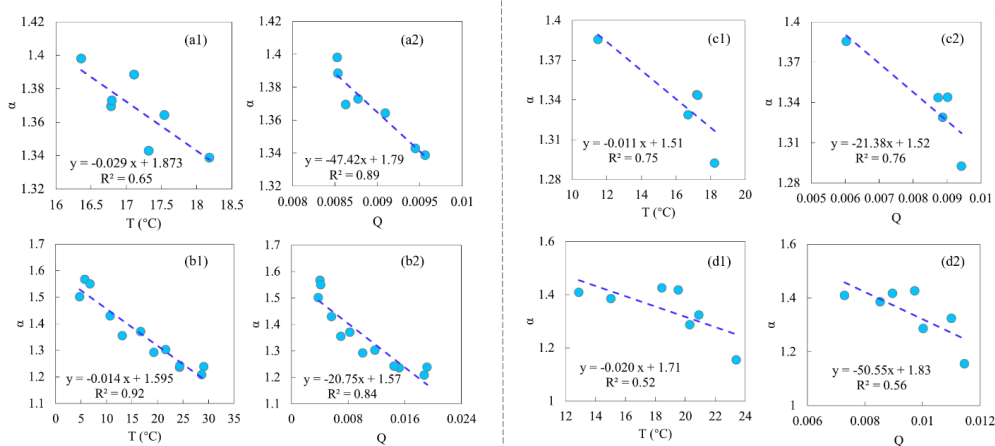


FGOALS-g3	China	CAS
FIO-ESM-2-0	China	CAS
MPI-ESM1-2-HR	Germany	DKRZ; DWD; MPI-M
MPI-ESM1-2-LR	Germany	MPI-M
NorESM2-LM	Norway	NCC
NorESM2-MM	Norway	NCC

## 219 3.2 Results

### 220 (1) Temporal and spatial changes in $\alpha$

221 We used yearly and climatology monthly (from Jan to Dec) data from Lake Taihu to  
 222 investigate the temporal variation in  $\alpha$ .  $\alpha$  is firstly inversed by the PT model and  
 223 measurements, and then we found significant negative relationships of  $\alpha$  with both T and  
 224 Q (Figure 4). On the yearly scale, the regressed values of  $da/dT$  and  $da/dQ$  are -  
 225  $0.029/^\circ\text{C}$  and  $-47.42$ , and the values on the seasonal scale are  $-0.014/^\circ\text{C}$  and  $-20.75$ ,  
 226 respectively.  $da/dT$  on the seasonal scale is higher than that on the yearly scale because  
 227 the variation range of  $\alpha$  on the seasonal scale is more extensive. Theoretical derived  $da/dT$   
 228 and  $da/dQ$  roughly match with the regressed values (Table 3).



229

230 Figure 4. Temporal and spatial relationships of  $\alpha$  and temperature (T) and specific  
 231 humidity (Q). (a-b) Temporal relationships based on lake Taihu data: (a) yearly data, and  
 232 (b) climatology monthly data. (c-d) Spatial relationships: (c) data from five water surface  
 233 sites, and (d) land surface data from FluxNet2015, each circle representing one vegetation  
 234 type. The linear regression line and correlation coefficient ( $R^2$ ) are shown in each  
 235 subpanel.

236

237 Table 3 Sensitivity of  $\alpha$  to temperature (T) and specific humidity (Q) by regression and



238 theoretical derivation.

		d $\alpha$ /dT (/°C)		d $\alpha$ /dQ	
		regression	derivation	regression	derivation
Temporal	yearly	-0.029	-0.023	-47.42	-37.95
	seasonally	-0.014	-0.011	-20.75	-18.38
Spatial	water sites	-0.011	-0.012	-21.38	-24.30
	land sites	-0.020	-0.016	-50.55	-40.47

239

240 Spatial relationships of  $\alpha$  with T and Q are similar to that in time, i.e., higher T and Q  
 241 generally correspond to lower  $\alpha$ , supported by measurements over both water and land  
 242 surfaces (Figure 4). For the water surfaces, the values of d $\alpha$ /dT and d $\alpha$ /dQ are -  
 243 0.011/°C and -21.38, and the values for land surfaces are -0.020/°C and -50.55. The  
 244 derived d $\alpha$ /dT and d $\alpha$ /dQ reasonably match well with the regressed values (Table 3).  
 245 The correlations (represented by R<sup>2</sup> in Figure 4) between  $\alpha$  and T,  $\alpha$  and Q of water  
 246 surfaces are higher than those over the land surfaces. This indicates that changes in  $\alpha$   
 247 are more associated with T and Q over water surfaces, which may be because T and Q  
 248 dominate the water surface evaporation process, while some other factors, like vegetation  
 249 and wind speed, also play specific roles over land surfaces.

250 Based on Equation (20) to (22),  $\partial\alpha/\partial T$  is always a negative value, and  $\partial\alpha/\partial Q$  is  
 251 always positive. The regressed and derived d $\alpha$ /dT and d $\alpha$ /dQ are both negative.  
 252 Combined with Equations (24), (25) and the positive relationship between T and Q, the  
 253  $\partial\alpha/\partial T$  plays a more critical role in determining (the signs of) d $\alpha$ /dT and d $\alpha$ /dQ, that  
 254 is,  $|\partial\alpha/\partial T| > \partial\alpha/\partial Q \cdot dQ/dT$  and  $|\partial\alpha/\partial T \cdot dT/dQ| > \partial\alpha/\partial Q$ . Specifically, based on the data  
 255 from lake Taihu (for detecting  $\alpha$  changes in time) and data from different water surface  
 256 sites and land surface sites (for detecting  $\alpha$  changes in space), we found the contribution  
 257 of  $\partial\alpha/\partial T \cdot dT$  to d $\alpha$  is ~70%, much more significant than that of  $\partial\alpha/\partial Q \cdot dQ$  of ~30%  
 258 (Table 4). Therefore, according to the evaporation process over the wet surface (Section  
 259 2.1) and the above analyses, we can conclude that  $\alpha$  is fundamentally controlled by T and  
 260 modulated by Q.

261 Table 4. Contributions of changes in temperature (T) and specific humidity (Q) to  
 262 changes in  $\alpha$ .

		d $\alpha$	contribution of $\frac{\partial\alpha}{\partial T} dT$	contribution of $\frac{\partial\alpha}{\partial Q} dQ$
Temporal	yearly	-0.035	78%	22%
	seasonally	-0.256	67%	33%
Spatial	water sites	-0.081	68%	32%
	land sites	-0.167	77%	23%
Average		----	72.5%	27.5%



263 Note: Since  $d\alpha = \frac{\partial\alpha}{\partial T}dT + \frac{\partial\alpha}{\partial Q}dQ$ , the contribution of  $\frac{\partial\alpha}{\partial T}dT$  is calculated as

264  $\left| \frac{\partial\alpha}{\partial T}dT \right| / \left| \frac{\partial\alpha}{\partial T}dT + \frac{\partial\alpha}{\partial Q}dQ \right|$ , and is the contribution of  $\frac{\partial\alpha}{\partial Q}dQ$  calculated as

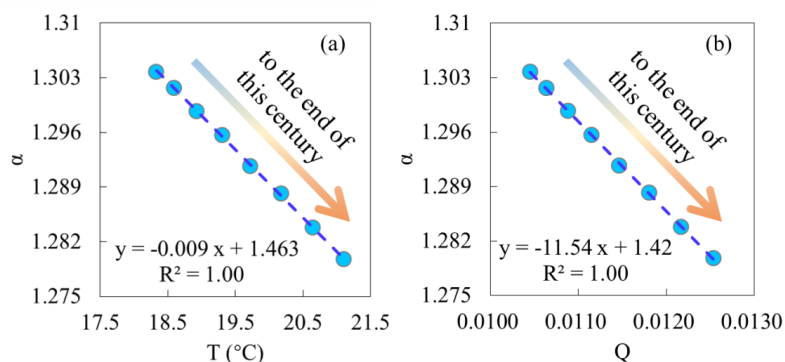
265  $\left| \frac{\partial\alpha}{\partial Q}dQ \right| / \left| \frac{\partial\alpha}{\partial T}dT + \frac{\partial\alpha}{\partial Q}dQ \right|$ .  $d\alpha$  refers to the estimated variation of  $\alpha$  from lowest to highest

266 T (also from lowest to highest Q since T and Q are positively correlated).

267 Derived  $d\alpha/dT$  and  $d\alpha/dQ$  have more or less errors compared to the regressed values.  
268 Several reasons can explain this: (i) errors in measurements of eddy covariance systems;  
269 (ii) the additional factors other than T and Q, like wind speed, can also influence  $\alpha$ ; (iii)  
270 the relationship of  $\alpha$  and T (also  $\alpha$  and Q) cannot be well represented by the linear  
271 regression model. Besides, the water surface size effects on evaporation and  $\alpha$ , reported  
272 by Han and Guo (2023), are not well considered in the presented derivation. Nevertheless,  
273 the derived expression can fairly match the observations of water bodies with various  
274 sizes (Table 3).

## 275 (2) Potential applications for global projections

276 Based on CMIP6 ocean surface data, we also detected significant negative relationships  
277 of  $\alpha$  with T and Q (Figure 5).  $d\alpha/dT$  and  $d\alpha/dQ$  obtained by the linear regression are -  
278 0.009/°C and -11.54, respectively. The derived  $d\alpha/dT$  and  $d\alpha/dQ$  are close to the  
279 regressed value as -0.009/°C and -10.74. We further compared the changes in T, Q, and  
280 heat fluxes between the first and the last ten years in 2021-2100 (Table 5). To the end of  
281 this century, CMIP6 models predict that ocean average available energy ( $R_n-G$ ) and latent  
282 heat flux (also evaporation) will increase by  $\sim 3.1$  W/m<sup>2</sup> and  $\sim 6.0$  W/m<sup>2</sup>, respectively.  
283 Using the PT model with the fixed  $\alpha$  (1.26), predicted evaporation shows an increase of  
284  $\sim 8.0$  W/m<sup>2</sup>, far higher than climate models' direct output (with a relative bias of  $\sim 30\%$ ).  
285 Based on derived  $\alpha$ , ocean evaporation shows a much smaller increase of  $\sim 5.8$  W/m<sup>2</sup>, with  
286 less than 5% relative bias compared to CMIP6 values (Figure 6). This indicates that  
287 changes in  $\alpha$  should be well considered for the long-term projections. So here we suggest  
288 introducing the negative relationship between  $\alpha$  and T, proposed in this study, into the  
289 original PT model to correct for the overestimated sensitivity of evaporation to  
290 temperature (Liu *et al.*, 2022), which could also improve the reliability of global long-  
291 term drought predictions (Greve *et al.*, 2019).



292

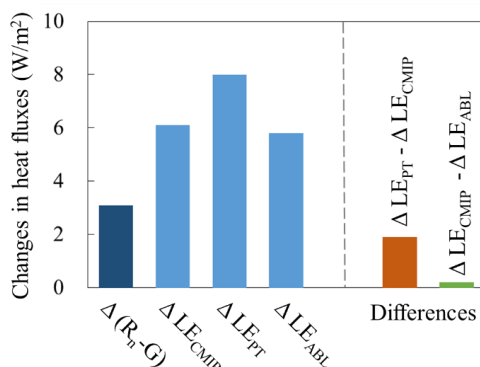
293 Figure 5. Temporal relationship of (a)  $\alpha$  and temperature (T), and (b)  $\alpha$  and specific  
 294 humidity (Q) over global ocean surfaces. Each dot denotes the data in each 10-year  
 295 window (2021-2030, 2031-2041, ..., 2091-2100), from left to right is from 2021-2030 to  
 296 2091-2100.

297

298 Table 5. Ocean surface temperature, specific humidity, and heat fluxes at the first ten  
 299 years (2021-2030) and the end of the 21<sup>st</sup> century (2091-2100). T, Q,  $R_n-G$ , and LE are  
 300 direct outputs of climate models.  $\alpha$ -CMIP refers to  $\alpha$  inverted by the PT model with CMIP  
 301 data.  $LE_{PT}$  is calculated by the PT model with fixed  $\alpha$  at 1.26.  $\alpha$ -ABL refers to  $\alpha$  estimated  
 302 by the ABL model.  $LE_{ABL}$  is calculated by the PT model with  $\alpha$ -ABL.

Period	T (°C)	Q (-)	$R_n-G$ (W/m <sup>2</sup> )	LE (W/m <sup>2</sup> )	$\alpha$ -CMIP	$LE_{PT}$ (W/m <sup>2</sup> )	$\alpha$ -ABL	$LE_{ABL}$ (W/m <sup>2</sup> )
2021-2030	18.1	0.010	122.9	106.8	1.304	103.2	1.316	107.7
2091-2100	21.1	0.013	126.0	112.9	1.279	111.2	1.287	113.5
$\Delta$	3.0	0.003	3.1	6.1	-0.025	8.0	-0.029	5.8

303



304

305 Figure 6. Stylized diagram showing the average changes in heat fluxes over global  
 306 ocean surfaces.



#### 307 4. Discussions and Conclusions

308 An atmospheric boundary layer model, built initially on Liu and Yang (2021), was used  
309 to derive an expression for the Priestley-Taylor coefficient,  $\alpha$ . The expression explicitly  
310 shows the dependences of  $\alpha$  on air temperature and specific humidity. Temperature  
311 changes dominate changes in  $\alpha$ , compared to specific humidity. We suggest that for the  
312 study focusing on evaporation and/or drought projections, the negative relationship  
313 between  $\alpha$  and temperature should be well characterized, which can be calculated by the  
314 proposed expression.

315 It should be noted that except for the PT model, the PM-based model can be also used to  
316 estimate wet surface evaporation (Penman, 1948; Shuttleworth, 1993). While PM-based  
317 equations encapsulate all processes that possibly affect evaporation, the PT model, taking  
318 evaporation as a simple function of radiation and temperature, takes more account of the  
319 feedback/balance between the surface and near atmosphere (Figure 1). Besides, it has  
320 been noted that the PM-based models may fail at certain limits, and cannot capture the  
321 sensitivity of evaporation to temperature changes (Liu et al., 2022; McColl, 2020). So in  
322 this case, also with the fact that the PT model is currently one of the most popular  
323 equations due to its low input requirements, revisiting this classic model can greatly  
324 promote its adaption under the changing climate.

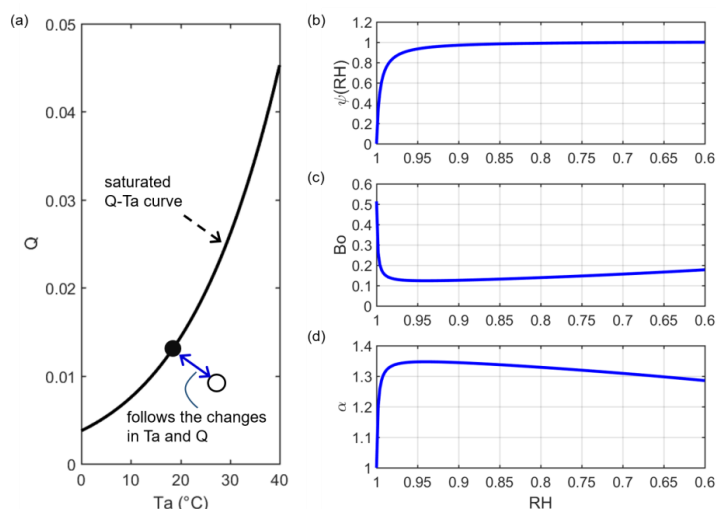
325 In Section 2.1, it was suggested that  $\Delta_D = 0$  for the equilibrium state while  $\Delta_D \approx Q$  for  
326 the non-equilibrium state. In theory, it is expected that the transition track between  
327 equilibrium and non-equilibrium states should be continuous and smooth. That is, the  
328 changes in the value of  $\Delta_D$  between the equilibrium state (0) and non-equilibrium state  
329 (Q) should follow the variations in air energy and moisture (Figure 7 (a)). Since the  
330 relative humidity (RH) includes both information on air temperature and humidity, here  
331 we introduce a possible track of  $\Delta_D$  depending on RH as:  $\Delta_D = \psi(\text{RH}) \cdot Q$ . As we expect,  
332 the value of  $\Delta_D$  approaches 0 when the air is very moist (i.e., very close to the equilibrium  
333 state and RH close to 1), so  $\psi$  should be a nonlinear and monotone convex function of  
334 RH. We give a possible expression of  $\psi(\text{RH})$  as:

$$335 \quad \psi(\text{RH}) = 1 - \frac{1}{1 + m \times \left( \frac{\text{RH}_{\max} - \text{RH}}{\text{RH} - \text{RH}_{\min}} \right)^n} \quad (28)$$

336 where  $\text{RH}_{\max}$  is 1, and  $\text{RH}_{\min}$  is 0.6 (McColl and Tang, 2023) over the water surfaces.  $m$   
337 and  $n$  are shape parameters. To make  $\psi(\text{RH})$  simple, we fixed  $n$  at 1, and let  $m$  be 100.  
338 The relationship between  $\psi(\text{RH})$  and RH can be viewed in Figure 7 (b). For a specific  
339 case that  $T$  at 18 °C, we show the changes in  $\text{Bo}$  and  $\alpha$  with RH in Figure 7 (c)-(d).  
340 Although there is a dramatic shift in  $\text{Bo}$  or  $\alpha$ , it appears when RH is at 0.95-1, which is



341 outside the vast majority of actual cases (RH is generally smaller than 0.9 on a monthly  
342 or longer scale). After the shift point, with RH decreases,  $\psi(\text{RH})$ ,  $B_0$ , and  $\alpha$  remain  
343 roughly stable. It is worth noting that Equation (28) (with specific parameters) is one  
344 possible case that connects the transition between equilibrium and non-equilibrium states,  
345 a fine determination may be affected by local conditions, but  $\Delta_D$  value around  $Q$  is  
346 expected for most of the cases.



347  
348 Figure 7. (a) Transition between equilibrium and non-equilibrium states. The filled circle  
349 represents one case in which the air is saturated (equilibrium state) and the open circle  
350 represents one case in which air is not saturated (non-equilibrium state). (b) Relationship  
351 between  $\psi(\text{RH})$  and RH with Equation (28). (c)-(d) Changes in  $B_0$  and  $\alpha$  as the  
352 function of RH when air temperature is fixed at 18 °C.

353 The derived formula for  $\alpha$  has important practical meanings. For example, it would be  
354 useful for estimating water surface evaporation and actual evapotranspiration based on  
355 the PT model (Maes *et al.*, 2019; Miralles *et al.*, 2011). It can also help to constrain the  
356 relationships among  $\alpha$ ,  $T$ , and  $Q$  in the complementary relationship, whose performance  
357 previously depended on the inversed  $\alpha$  (Liu *et al.*, 2016). Besides, considering the impacts  
358 of changing climate on  $\alpha$  can significantly improve the performance of the hydrologic  
359 model in runoff simulations and predictions (Pimentel *et al.*, 2023).

### 360 Author Contributions

361 Conceptualization: Ziwei Liu, Hanbo Yang. Data curation: Ziwei Liu. Formal analysis:  
362 Ziwei Liu. Funding acquisition: Hanbo Yang. Methodology: Ziwei Liu, Hanbo Yang.  
363 Software: Ziwei Liu. Supervision: Hanbo Yang. Writing – original draft: Ziwei Liu.



364 Writing – review & editing: Changming Li, Taihua Wang, Hanbo Yang.

365 **Data availability**

366 Data of Lake Taihu can be obtained from Harvard Dataverse,  
367 <https://doi.org/10.7910/DVN/HEWCWM>. The data of Poyang Lake can be obtained  
368 from Zhao and Liu (2018) and Gan and Liu (2020). The data of Erhai can be obtained  
369 from Du *et al.* (2018). The data of Guandu can be obtained from Zhao *et al.* (2019). The  
370 data of Suwa lake can be obtained from the AsiaFlux  
371 ([http://asiaflux.net/index.php?page\\_id=1355](http://asiaflux.net/index.php?page_id=1355)). FluxNet 2015 data are available at  
372 <https://fluxnet.fluxdata.org/data/download-data/>. CMIP6 data can be obtained from  
373 Earth System Grid Federation (<https://esgf-node.llnl.gov>).

374 **Acknowledgments**

375 This study is financially supported by the National Natural Science Foundation of China  
376 (grant nos. 51979140, 42041004).

377 **Competing interests**

378 No competing interests.



379 **References:**

- 380 Andreas, E. L., and B. A. Cash (1996), A new formulation for the Bowen ratio over saturated surfaces,  
381 *Journal of Applied Meteorology*, 35(8), 1279-1289.
- 382 Assouline, S., D. Li, S. Tyler, J. Tanny, S. Cohen, E. Bou-Zeid, M. Parlange, and G. G. Katul (2016), On  
383 the variability of the Priestley-Taylor coefficient over water bodies, *Water Resources Research*, 52(1), 150-  
384 163.
- 385 Bowen, I. S. (1926), The ratio of heat losses by conduction and by evaporation from any water surface,  
386 *Physical Review*, 27(6), 779-787.
- 387 Brutsaert, W., and H. J. W. r. r. Stricker (1979), An advection-aridity approach to estimate actual regional  
388 evapotranspiration, 15(2), 443-450.
- 389 Crago, R. D., J. Szilagyi, and R. J. Qualls (2023), What is the Priestley–Taylor wet-surface evaporation  
390 parameter? Testing four hypotheses, *Hydrol. Earth Syst. Sci.*, 27(17), 3205-3220.
- 391 Debruin, H. A. R., and J. Q. Keijman (1979), PRIESTLEY-TAYLOR EVAPORATION MODEL APPLIED  
392 TO A LARGE, SHALLOW LAKE IN THE NETHERLANDS, *Journal of Applied Meteorology*, 18(7),  
393 898-903.
- 394 Du, Q., H. Z. Liu, Y. Liu, L. Wang, L. J. Xu, J. H. Sun, and A. L. Xu (2018), Factors controlling evaporation  
395 and the CO<sub>2</sub> flux over an open water lake in southwest of China on multiple temporal scales, *International*  
396 *Journal of Climatology*, 38(13), 4723-4739.
- 397 Eichinger, W. E., M. B. Parlange, and H. Stricker (1996), On the concept of equilibrium evaporation and  
398 the value of the Priestley-Taylor coefficient, *Water Resources Research*, 32(1), 161-164.
- 399 Gan, G., and Y. Liu (2020), Heat Storage Effect on Evaporation Estimates of China's Largest Freshwater  
400 Lake, 125(19), e2019JD032334.
- 401 Greve, P., M. L. Roderick, A. M. Ukkola, and Y. Wada (2019), The aridity Index under global warming,  
402 *Environmental Research Letters*, 14(12).
- 403 Guo, X., H. Liu, and K. J. B.-L. M. Yang (2015), On the application of the Priestley–Taylor relation on sub-  
404 daily time scales, 156, 489-499.
- 405 Han, S., and F. Guo (2023), Evaporation From Six Water Bodies of Various Sizes in East Asia: An Analysis  
406 on Size Dependency, *Water Resources Research*, 59(6).
- 407 Hicks, B. B., and G. D. Hess (1977), On the Bowen Ratio and Surface Temperature at Sea, *Journal of*  
408 *Physical Oceanography*, 7(1), 141-145.
- 409 Jury, W., and C. J. A. J. Tanner (1975), Advection Modification of the Priestley and Taylor  
410 Evapotranspiration Formula 1, 67(6), 840-842.
- 411 Lee, X., S. Liu, W. Xiao, W. Wang, Z. Gao, C. Cao, C. Hu, Z. Hu, S. Shen, Y. Wang, X. Wen, Q. Xiao, J.  
412 Xu, J. Yang, and M. Zhang (2014), THE TAIHU EDDY FLUX NETWORK An Observational Program on  
413 Energy, Water, and Greenhouse Gas Fluxes of a Large Freshwater Lake, *Bulletin of the American*  
414 *Meteorological Society*, 95(10), 1583-1594.
- 415 Lhomme, J. P. (1997a), An examination of the Priestley-Taylor equation using a convective boundary layer  
416 model, *Water Resources Research*, 33(11), 2571-2578.
- 417 Lhomme, J. P. (1997b), A theoretical basis for the Priestley-Taylor coefficient, *Boundary-Layer*  
418 *Meteorology*, 82(2), 179-191.
- 419 Liu, X., C. Liu, and W. Brutsaert (2016), Regional evaporation estimates in the eastern monsoon region of  
420 China: Assessment of a nonlinear formulation of the complementary principle, 52(12), 9511-9521.



- 421 Liu, Z., and H. Yang (2021), Estimation of Water Surface Energy Partitioning With a Conceptual  
422 Atmospheric Boundary Layer Model, *Geophysical Research Letters*, 48(9), e2021GL092643.
- 423 Liu, Z., J. Han, and H. Yang (2022), Assessing the ability of potential evaporation models to capture the  
424 sensitivity to temperature, *Agricultural and Forest Meteorology*, 317, 108886.
- 425 Maes, W. H., P. Gentine, N. E. C. Verhoest, and D. G. Miralles (2019), Potential evaporation at eddy-  
426 covariance sites across the globe, *Hydrology and Earth System Sciences*, 23(2), 925-948.
- 427 McColl, K. A., and L. I. Tang (2023), An analytic theory of near-surface relative humidity over land,  
428 *Journal of Climate*.
- 429 McNaughton, K., and T. Spriggs (1986), A MIXED-LAYER MODEL FOR REGIONAL EVAPORATION,  
430 *Boundary-Layer Meteorology*, 34(3), 243-262.
- 431 Miralles, D. G., T. Holmes, R. De Jeu, J. Gash, A. Meesters, A. J. H. Dolman, and E. S. Sciences (2011),  
432 Global land-surface evaporation estimated from satellite-based observations, 15(2), 453-469.
- 433 Penman, H. L. (1948), Natural evaporation from open water, bare soil and grass, *Proceedings of the Royal  
434 Society of London Series a-Mathematical and Physical Sciences*, 193(1032), 120-145.
- 435 Pimentel, R., B. Arheimer, L. Crochemore, J. C. M. Andersson, I. G. Pechlivanidis, and D. Gustafsson  
436 (2023), Which Potential Evapotranspiration Formula to Use in Hydrological Modeling World-Wide?, 59(5),  
437 e2022WR033447.
- 438 Priestley, C. H. B., and R. J. Taylor (1972), Assessment of surface heat-flux and evaporation using large-  
439 scale parameters, *Monthly Weather Review*, 100(2), 81-92.
- 440 Raupach, M. R. (2001), Combination theory and equilibrium evaporation, *Quarterly Journal of the Royal  
441 Meteorological Society*, 127(574), 1149-1181.
- 442 Roderick, M. L., F. Sun, W. H. Lim, and G. D. Farquhar (2014), A general framework for understanding  
443 the response of the water cycle to global warming over land and ocean, *Hydrology and Earth System  
444 Sciences*, 18(5), 1575-1589.
- 445 Shuttleworth, W. J. (1993), *Evaporation In: Maidment, DR Handbook of hydrology*, edited, McGraw-Hill  
446 New York.
- 447 Slatyer, R. O., and I. C. McIlroy (1961), *Practical microclimatology: with special reference to the water  
448 factor in soil-plant-atmosphere relationships*, Melbourne: Commonwealth Scientific and Industrial  
449 Research Organisation.
- 450 Su, Q., and V. P. Singh (2023), Calibration-Free Priestley-Taylor Method for Reference Evapotranspiration  
451 Estimation, 59(3), e2022WR033198.
- 452 Taoka, T., H. Iwata, R. Hirata, Y. Takahashi, Y. Miyabara, and M. Itoh (2020), Environmental Controls of  
453 Diffusive and Ebullitive Methane Emissions at a Subdaily Time Scale in the Littoral Zone of a Midlatitude  
454 Shallow Lake, *Journal of Geophysical Research-Biogeosciences*, 125(9).
- 455 Thornthwaite, C. W., and B. Holzman (1939), Evaporation from land and water surfaces, *Monthly Weather  
456 Review*, 67, 4-11.
- 457 van Heerwaarden, C. C., J. V. G. de Arellano, A. F. Moene, and A. A. M. Holtslag (2009), Interactions  
458 between dry-air entrainment, surface evaporation and convective boundary-layer development, *Quarterly  
459 Journal of the Royal Meteorological Society*, 135(642), 1277-1291.
- 460 Xiao, W., Z. Zhang, W. Wang, M. Zhang, Q. Liu, Y. Hu, W. Huang, S. Liu, and X. Lee (2020), Radiation  
461 Controls the Interannual Variability of Evaporation of a Subtropical Lake, *Journal of Geophysical  
462 Research-Atmospheres*, 125(8).
- 463 Yang, Y., and M. L. Roderick (2019), Radiation, surface temperature and evaporation over wet surfaces,  
464 *Quarterly Journal of the Royal Meteorological Society*, 145(720), 1118-1129.
- 465 Zhao, J., M. Zhang, W. Xiao, W. Wang, Z. Zhang, Z. Yu, Q. Xiao, Z. Cao, J. Xu, X. Zhang, S. Liu, and X.



466 Lee (2019), An evaluation of the flux-gradient and the eddy covariance method to measure CH<sub>4</sub>, CO<sub>2</sub>, and  
467 H<sub>2</sub>O fluxes from small ponds, *Agricultural and Forest Meteorology*, 275, 255-264.  
468 Zhao, X., and Y. Liu (2018), Variability of Surface Heat Fluxes and Its Driving Forces at Different Time  
469 Scales Over a Large Ephemeral Lake in China, *Journal of Geophysical Research-Atmospheres*, 123(10),  
470 4939-4957.

471